Available online at www.sciencedirect.com

ScienceDirect

Procedia Computer Science 232 (2024) 2072–2081

Procedia Computer Science

www.elsevier.com/locate/procedia

5th International Conference on Industry 4.0 and Smart Manufacturing

Software compensation to improve the Stereolithography fabrication of porous features and porous surface texturing at micro-scale

Vito Basile[a,*], Francesco Modica[a], Irene Fassi[b]

[a] CNR-STIIMA Institute of Intelligent Industrial Technologies and Systems for Advanced Manufacturing, Via P. Lembo, 38F, Bari, 70124, Italy
[b] CNR-STIIMA Institute of Intelligent Industrial Technologies and Systems for Advanced Manufacturing, Via A. Corti, 12, Milano, 20133, Italy

Abstract

Nano and micro-porous structures exhibit intriguing properties for a wide variety of applications, spanning from the biomedical to sensing. However, their fabrication is a challenge in terms of dimensional accuracy, which affects devices' performance and sensitivity. In this paper, we present a route to enhance the dimensional accuracy of fabrication via Stereolithography (SLA) of porous features at the micro-scale. Using a custom benchmark part, deviations in feature dimensions (micro-pores diameters and depths) were measured by confocal microscopy. Sample characterization and experimental observations allowed the identification of inaccuracy sources (i.e., laser spot size and its compensation on path generation), and a compensation method of the nominal laser spot diameter (85μm) was defined. Implementing such a method results in relevant improvements in dimensional accuracy: 9.8% and 11.3% on full-open pores diameter and depth, respectively. Partially open pores accuracy improvements were 15.8% on diameters and 1.5% on depths. Since machine optical equipment can result in deviations in the actual laser spot diameter from the nominal value, the actual laser beam spot diameter was estimated by printing a test part and adopting this information to adjust a calibration procedure. The measurements revealed that the actual laser beam spot size is 93±8μm. The proposed method can be extended for the fabrication of any micro-porous structures.

Keywords: Additive Manufacturing; Stereolithography; Surface micro-texturing; Micro-features; Micro-pores; Surface functionalization; Functionally graded materials.

* Corresponding author. Tel.: +39-080-5481265.
E-mail address: vito.basile@stiima.cnr.it

1877-0509
10.1016/j.procs.2024.02.143

1. Introduction

Porous materials have a great potential for many applications [1], due to their unique properties: they are lightweight, exhibit peculiar mechanical properties and behavior, liquid and gas/vapor absorption, permeability, wettability and, hydrophilicity, etc. [1, 2]. These materials are made of a base material (matrix) such as ceramics, metals, polymers, elastomers, composites, etc., with voids or pores distributed on their surface or volume. According to this generic definition, porous materials are sintered powders, foams, sponges, lattice structures, etc.

Their applications are wide: 1) Gas/air and fluids filtration and treatment; 2) energy storage and conversion (super capacitor, fuel cell, batteries); 3) biomedical; 4) Sensors and more. Some relevant medical applications are scaffold to enable and promote in-vitro cell culture, in-vivo tissue-induced regeneration, specialized human tissue substitutions and prosthesis, foams for drug delivery, diagnostic and sensing, and 3D culture platforms for cancer response to drugs [3]. Finally, some geometrical and topological 3D structures, i.e., inverse opal, thus face-cubic-centered (FCC) structures, are photonic crystals, and they exhibit unique light processing capability [4] or behave as shape memory polymers [5]. Porous material properties depend on the base material properties and on the geometrical characteristics: 1) pores geometry, type (open/closed), pore sizes and distribution (ordered/regular or random); 2) pores network connections. The main traditional manufacturing technologies suitable for porous materials production are sintering of powders, die casting of metal foams, chemical reactions in polymer, elastomers, and composites processing technologies such as compression and injection molding, extrusion, etc. All these technologies are affordable and capable of complex shapes, but they suffer of poor process control capability since they do not allow the fabrication of products with demanding requirements for high-performance applications [6]. In addition, they do not allow the fabrication of highly ordered/regular porous structures, such as lattice structures, close-packed opals, and inverse opals, scaffolds (i.e., woodpile, opal, and inverse opal), etc. Additive manufacturing (AM) technologies are capable of highly complex geometry fabrications of products made of a wide variety of materials, with high process control, high dimensional accuracy and surface finishing. Among AM technologies, Stereolithography (SLA), belonging to the family of Vat Photopolymerization (VPP) technologies, is one of the most successful due to its performance, high speed, resolution, high precision, smooth finishing, low waste, and affordability of polymers, composites and ceramics materials, with a fully-digitalized process [7]. The SLA can be successfully used to fabricate regular/high-ordered porous structures [8, 9]. Figure 1 shows an inverse opal FCC structure fabricated via bottom-up SLA.

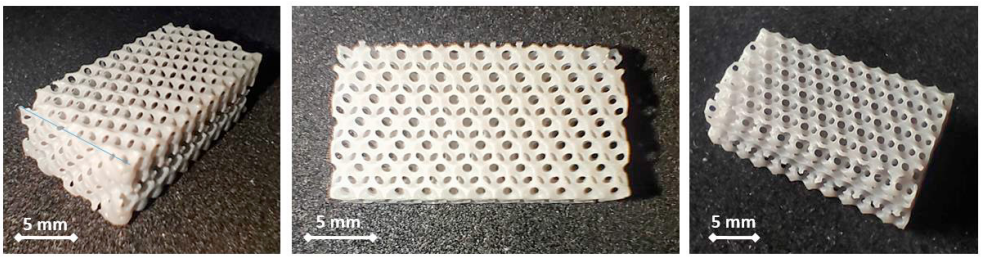

Fig. 1. Samples of inverse opal FCC porous structure fabricated via Stereolithography. Nominal pore diameter D=2mm.

A higher accuracy in fabrication is possible by several AM technologies with direct effects on the device quality of high-added value sectors [10]. Due to its relevant capabilities, SLA process with its variants (top-down and bottom-up exposure) attracted the scientific community's interest. Several studies were conducted with different objectives: development of advanced applications, process parameters optimization, exploration of new materials performance and processability, addressing technology issues and limitations, conceiving innovative process chains, etc. [8-13]. Remarkable achievements were obtained by investigating SLA process parameters aiming at identifying their effects on the 3D-printed part quality: dimensional accuracy, surface finishing, mechanical properties, defects occurrence, etc. Sabbah A. et al. [14] found a negligible impact of the layer thickness on surface finishing, while it strongly affects the dimensional accuracy of 3D-printed parts. The minimum layer thickness of 25 μm resulted in higher precision.

Arnold C. et al. [15] concluded that the surface roughness of 3D-printed parts is firmly dependent on the model orientation in the build volume. The best results were obtained with a 0-degree part orientation (horizontally on the

build platform) with measured values of Ra=1.15±0.47 μm along the X-axis and Ra=0.90±0.33 μm along the Y-axis. Other similar studies confirmed these results [16]. Shanmugasundaram S. et al. investigated the effects of printing orientation on the part's mechanical properties, and no significant anisotropy was detected thanks to UV-curing post-processing [17]. Cotabarren I. et al., confirmed that layer thickness is a critical parameter for part accuracy; measurement deviation was reduced by about 90% when this parameter was reduced from 100 to 25μm [18]. Hada, T. et al. found that the highest dimensional accuracy is achieved by orienting the part with a 45-degree angle on the build platform, followed by a 90-degree orientation. The worst orientation is the 0-degree with the part parallel to the build platform [19]. These results were also confirmed by other studies [20, 21]. As it can be noticed, several works focused on the influence of process parameters on the quality of 3D-printed parts, but there is a lack of research studies on the effects of the laser beam (i.e., laser spot size) and the quality of the scan path generation (preprocessing).

Since this technology is based on liquid photopolymers, which are polymerized by a laser beam spot (LBS) that scans and UV-cures the layer, the 3D-printed part's accuracy is strongly affected by the LBS size and scanning path, especially at the micro-scale. Focusing on these two factors, the actual size of the LBS and the scanning strategy adopted to UV-cure the current layer can be sources of relevant inaccuracy; thus, issues to be addressed.

In this work, we investigate the manufacturing of micro-pores features and structures via SLA technology by addressing the mentioned issues, which also determine relevant deviation in open pores size and shape. The technology limitations in micro-pores manufacturing is evaluated, and an effective solution is proposed, thus increasing the SLA capability and accuracy of the fabrication of this challenging structure.

2. Materials and methods

In this work, samples were fabricated with a Formlabs Form 3 (Formlabs Inc., USA), having a build volume of 145×145×185 mm^3, equipped with a class 1 violet laser emitting at a wavelength of 405nm with a nominal laser beam spot diameter D_{LB} of 85 μm and a power of 250 mW. The positioning resolution on the x-y plane is 25 μm, while the z-axis resolution can be set from 200 to 25 μm (layer thickness). Samples were designed with the 3D CAD Solidworks 2017 (Solidworks Corp., Dassault Systèmes, USA), exported to Stereo Lithography interface (STL) format and then imported into the Formlabs slicing software Preform v.3.29.1. In this software environment, parts were oriented and all the process parameters were chosen according to the database supplied by the machine manufacturer and to previous studies [11, 16, 22]. The surface with micro-pore features was oriented horizontally, thus parallel to the build platform, which guarantees a higher surface finishing [16, 22]. The main process parameters are reported in Table 1.

Table 1. SLA process parameters.

Parameter	Units	Values	Symbol
Layer Thickness	μm	25	LT
Support attachment point size	mm	0.7	APS
Support positions	-	Uniformly distributed	-
Support points density. Index (0.5-1.5)	-	1 (average 1.75 supports/10mm^2)	SPD
Base thickness	mm	2	BT
Min distance of the part from the base	mm	5	DPB
Part Orientations	deg	(0, 0, 0) Surface with horizontal pores	-

Samples were fabricated using a Formlabs Clear V04 photopolymer resin, identified by the manufacturer's code RS-F2-GPCL-04 [23]. After the SLA processing, parts were removed from the build platform and washed for 20 minutes into high-purity 99% isopropyl alcohol (IPA) and 5 minutes with ultrasound washing. The samples were, finally, UV-cured into the Formlabs Form Cure machine for 60 min at 60°C, according to the technical prescriptions of the resin supplier. Profiles and surface roughness of samples were acquired with a high-resolution optical profilometer Sensofar S Neox (Sensofar group, Barcellona, Spain), set with a confocal acquisition method.

2.1. Error source and software compensation method.

In order to investigate the effects of the laser beam path generation on the final part accuracy, a specific component, referred as Laser Path Evaluation Part (LPEP), was designed with both simple holes and protrusions. Figure 3 shows

the drawing of the part. The CAD model was then imported into the Formlabs Preform slicing software and the laser path generated. The LPEP was oriented flat on the build platform (horizontal, fig. 2, a) and preprocessed with the Preform algorithms to generate base, supports, slicing, and laser beam paths (fig. 2, b). Figure 3 reports the slicing and laser beam paths of holes (fig. 2, c, d) and protrusions (fig. 2, e, f). Looking at the generic slice of the region with holes, it can be easily recognized that the laser beam path starts exactly on the hole edge and it proceeds with a double-contour path of the 2D-slice geometry. This step of the layer curing strategy is also referred as the perimeter shell step. The bulk material, which is the external region of the hole, is then UV-cured by a rectilinear infill with parallel laser beam paths and a distance between them likely equal (or a bit smaller) to the laser spot diameter. The same observations can be made by looking at the protrusion features: the laser beam path contours the protrusion edges towards the material side with two contours, the first on the protrusion edge and the second with an offset from the first, and the internal region of the protrusion is filled with a rectilinear path oriented with a predefined angle (see fig. 2).

The hypothesis is the following. If the circular laser spot, having a diameter of D_{LS}, is centered on the line path, then all the edges of the slices, no matter if hollowed or protrusions will be affected by an over-polymerization equal to the laser spot radius. This will result in smaller holes and larger protrusions than nominal ones. Each laser spot polymerization of the current layer has a volume that can be approximated to $V_{LS}=D_{LS}*LT$. If the hypothesis is confirmed then an over-polymerized volume equal to R*LT will occur along the edge. Of course, at the meso and macro-scale, this inaccuracy is not relevant since it is a small percentage of the nominal dimensions, but it is very important at the micro-scale, where nominal dimensions are of the same (or close) order of the laser beam spot radius. The hypothesis is schematized in fig. 2, g) and h).

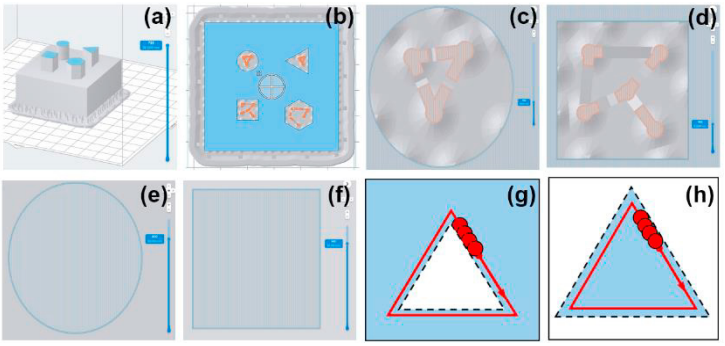

Fig. 2. Formlabs Preform slicing of the LPEP. (a) Part pre-processed into the virtual build volume; Images of a slice with holes (b, c, d) and protrusions (e, f). Hypothesis on layer UV-curing errors. Triangular hole (g) and protrusion (h). Nominal edges are depicted with a solid red line, also corresponding to the laser beam path; Actual UV-cured geometry (dashed black line); Bulk UV-cured region in blue color

If this hypothesis is confirmed, then inaccuracy occurs due to the missing compensation of the laser spot radius in the laser path generation algorithm, and a compensation method can be developed and applied. Since it is not possible to modify the laser path in the Preform slicing software, an effective strategy can be applying an offset volume at the 3D models, i.e., as a general rule, by increasing the cavities and by reducing protrusions. The correction to be applied should be carefully identified. In the simple case of spherical pore micro-features, the compensation to the model pore diameter is $D_P = D_{NP}+C$, where D_{NP} is the nominal pore diameter, and C is the compensation parameter. The first compensation value attempt is the nominal laser spot diameter supplied by the machine manufacturer $C=D_{LS}$.

2.2. Open micro-porous features

Micro-pore features are the fundamental component of all porous materials, as a single feature (1D), or which can be replicated in a surface texturing (2D planar or freeform pattern) or in a volume (3D). In the latter case, if the pores are regularly distributed along the three directions in a regular pattern, the resulting structures are lattices. All these cases are characterized by a single pore or a single cell, including pores and fractions of pores. For this reason, the proposed approach investigates the fabrication of a single pore and its accuracy. The investigation on the fabrication

by SLA of porous micro-features was performed by designing two sample sets:

1) Full-open pores (FOP), thus hemispherical cavities, with variable diameters from 1 mm (1-A) down to 0.5 mm (6-A) with a pitch of 100 μm (fig. 3, a);
2) Partially open pores (POP) with constant pore diameter D_P=1 mm and variable pore depth H (fig. 3, b), which result in variable pore aperture diameter D_{ANP}. In the latter case, depths were set to k=50, 65, 75 and 85% of the nominal pore diameter D_P. Table 2 reports the nominal dimensions of FOP and POP features.

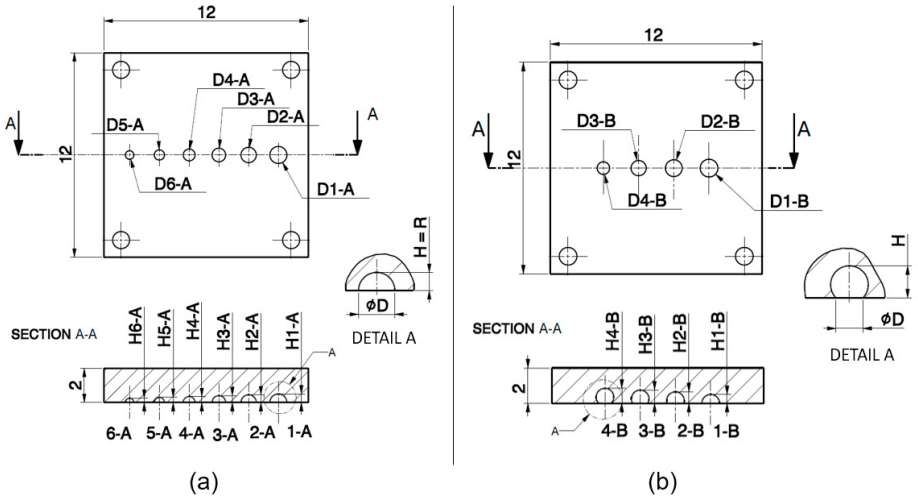

Fig. 3. (a) Full-open pores (FOP), depth equal to radius; (b) Partially-open pores (POP).

Table 2. Nominal dimensions of FOP and POP features (fig. 3).

Dimension (μm)	FOP Features #						POP Features #			
	1-A	2-A	3-A	4-A	5-A	6-A	1-B	2-B	3-B	4-B
D	1000	900	800	700	600	500	1000	954	866	714
H	500	450	400	350	300	250	500	650	750	850

$$\boldsymbol{D_{NAP} = 2 \cdot \sqrt{D_P \cdot (D_P - H) - (D_P - H)^2} = 2 \cdot D_P \cdot \sqrt{k\% \cdot (1 - k\%)}} \quad \text{where:} \quad \boldsymbol{H = k\% \cdot D_P} \qquad (1)$$

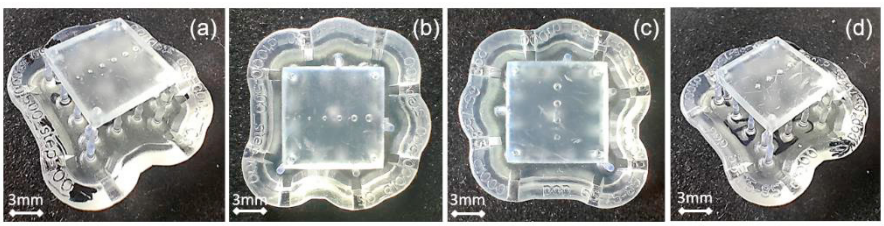

Fig. 4. Pictures of SLA fabricated samples: FOP (a, b) and POP (c, d).

The equation (1) gives the nominal value of the pore aperture diameters D_{NAP} with variable depths (see fig. 1, b, detail A). In this equation, the value of the pore diameter is constant D_P=1000 μm, while the depth H is set as a percentage k% of the diameter, H=k%*D_P. The values of k% were set to 50%, 65%, 75%, and 85%. Each geometry was realized in three samples with the same parameters reported in Table 1. Figure 4 shows the SLA fabricated samples before the detachment from the base and supports.

3. Results and discussion

Sections 3.1 and 3.2 present the measurements of the designed FOP and POP pore micro-features without and with compensation of the nominal laser beam spot diameter D_{LS}=85µm. Section 3.3 presents a method for the estimation of the actual compensation parameter C and its standard deviation, thus likely the actual laser beam spot diameter.

3.1. Measurements of full-open micro-pores (FOP)

The diameters and depths measurements of the full-open micro-pores are reported in Table 3 with their mean value and standard deviations; the same data are shown graphically in Fig. 5.

Table 3. Measurements of diameters and depths of the FOP.

PORE DIAMETER									PORE DEPTH								
Nominal	No Compensation				With Compensation				Nominal	No Compensation				With Compensation			
	Mean	STD	Average Error		Mean	STD	Average Error			Mean	STD	Average Error		Mean	STD	Average Error	
[µm]	*[µm]*	*[µm]*	*[µm]*	*[%]*	*[µm]*	*[µm]*	*[µm]*	*[%]*	*[µm]*	*[µm]*	*[µm]*	*[µm]*	*[%]*	*[µm]*	*[µm]*	*[µm]*	*[%]*
1000	907	22	-93	-9.3	975	18	-25	-2.5	500	465	4	-35	-7.0	503	5	3	0.6
900	808	16	-92	-10.2	869	57	-31	-3.4	450	413	8	-37	-8.2	444	9	-6	-1.3
800	689	42	-111	-13.9	763	6	-37	-4.6	400	349	12	-51	-12.8	388	11	-12	-3.0
700	592	30	-108	-15.4	653	23	-47	-6.7	350	265	20	-85	-24.3	318	2	-32	-9.1
600	468	16	-132	-22.0	530	7	-70	-11.7	300	157	36	-143	-47.7	231	5	-69	-23.0
500	365	31	-135	-27.0	461	14	-39	-7.8	250	71	11	-179	-71.6	147	6	-103	-41.2

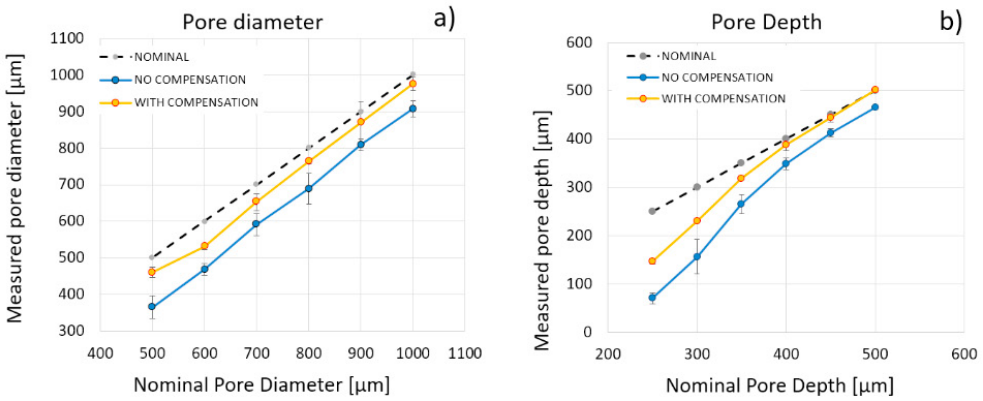

Fig. 5. Graphs of diameter (a) and depth (b) as a function of nominal values of the printed full-open micro-pores.

Considering the diameters of the pores, the average error spans between -92 and -135 µm. The average error is consistent (in value and sign) with the hypothesis of missing compensation of the laser beam spot radius. Further confirmation arises from the measured diameter considering a spot radius compensation (SRC) of 42.5µm, increasing the pore dimension accordingly. In this latter case, the error is reduced and spans between -25 and-75 µm. It is also possible to observe an increasing error trend when the diameter decreases. This behavior can be related to the fact that with the reduction of the diameter, it is more difficult to remove the resin from the cavity due to the adhesion on the solid surface (surface tension). Thus, the IPA washing aimed at removing uncured resin is less effective when the pore diameter decreases. This phenomenon prevents fabricating a few microns cavity and negatively affects the cavity, reducing its dimension proportionally to the drop size. At the same time, it is negligible for bigger cavities, with diameters in the order of a millimeter. The depth of the pores shows an average error that spans between -35 and -179µm, and the error is reduced when the SRC is adopted, varying between 3 and -103µm. The SRC has a beneficial influence on the depth error because it enlarges the cavity, producing two effects: it dampens the cutoff of the geometry slicing and reduces the resin adhesion effect.

3.2. Measurements of partially open micro-pores (POP)

In this test, four POPs with constant pore diameter D=1 mm were printed with variable pore depths (fig. 2, b), which results in variable pore aperture diameters. The pore diameters and depths of the POP measurements are reported in Table 4 with mean values and standard deviations, and the same data are shown graphically in fig. 6.

Table 4. Measurements of aperture diameters and depths of the POP.

PORE APERTURE DIAMETER									**PORE DEPTH**								
Nominal	No Compensation				With Compensation				Nominal	No Compensation				With Compensation			
	Mean	**STD**	**Average Error**		**Mean**	**STD**	**Average Error**			**Mean**	**STD**	**Average Error**		**Mean**	**STD**	**Average Error**	
[µm]	*[µm]*	*[µm]*	*[µm]*	*[%]*	*[µm]*	*[µm]*	*[µm]*	*[%]*	*[µm]*	*[µm]*	*[µm]*	*[µm]*	*[%]*	*[µm]*	*[µm]*	*[µm]*	*[%]*
1000	896	37	-104	-10.4	993	17	-7	-0.7	500	460	9	-40	-8.0	515	5	15	3.0
954	843	27	-111	-11.6	927	34	-27	-2.8	650	620	10	-30	-4.6	677	7	27	4.2
866	759	9	-107	-12.4	850	15	-16	-1.8	750	721	7	-29	-3.9	776	2	26	3.5
714	625	29	-89	-12.5	762	9	48	6.7	850	817	7	-33	-3.9	880	4	30	3.5

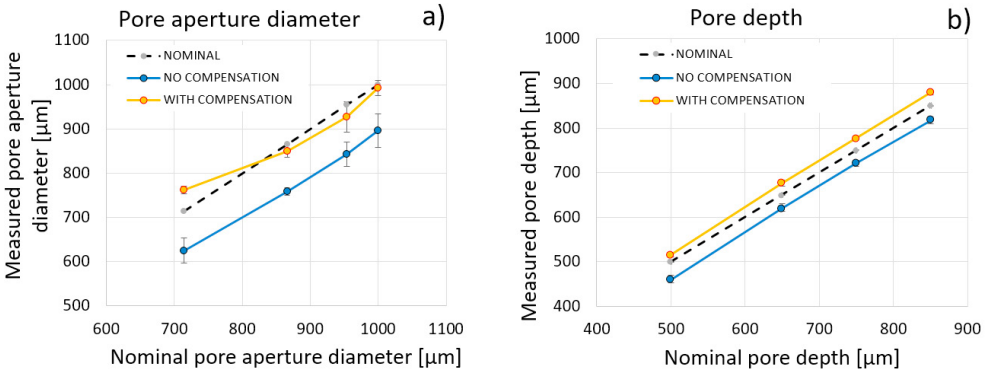

Fig. 6. Graphs of aperture diameter (a) and depth (b) as a function of nominal values of the printed partially-open micro-pores.

The aperture diameters of the no-compensated samples present an average error that spans between -89 and -111µm. The average error is consistent with the hypothesis of missing compensation of the laser beam spot radius. In fact, when adopting the SRC, the error is reduced in the range of -7 and +48µm, showing the compensation's effectiveness. On the contrary, the depths of the pores present a similar order of error for both no-compensated and with the SRC. The depth error for no-compensated pores is between -29 and -40µm with a light reduction when the depth is increased. Adopting SRC, the depth error is between 15 and 30µm, slightly increasing with the pore depth.

In this case, the SRC is less effective and changes the error sign. This is due the compensation method. Increasing the pore size by SRC results in increases in the pore depth. Considering that the resin adhesion effect is less significant for a pore diameter equal to or higher than 1mm, the vertical direction compensation should be reduced accordingly. Consequently, at this scale of pore size, a better approach is to apply the compensation mainly in the horizontal plane (slices), reducing or removing the compensation in the vertical direction.

3.3. Calibration procedure: Measurement of the compensation parameter

However, the actual value of the parameter C can be significantly different from the nominal value of the laser beam spot diameter due to the accuracy and quality of the optical equipment of the machine [24]. Therefore, to increase the final accuracy, it is necessary to use, in the proposed compensation approach, the actual laser spot size. To this aim, a part was designed (figure 7) with four repetitions of six squared thin wall features having variable wall thicknesses of 0.05, 0.1, 0.15, 0.2, 0.25, 0.17 mm. Thin wall thicknesses were chosen in the range 50-250µm with a pitch of 50µm. Since slicing always has two paths on each thin wall, a feature with a wall thickness equal to two times the laser beam spot nominal diameter (170µm) was added at the end of the pattern. Figure 7, a) shows the drawing of

the proposed part for the correction factor estimation. Samples were fabricated according to the described conditions (Section 2) and parameters (Table 1). A sample of the part is shown in Figure 7, b) and c).

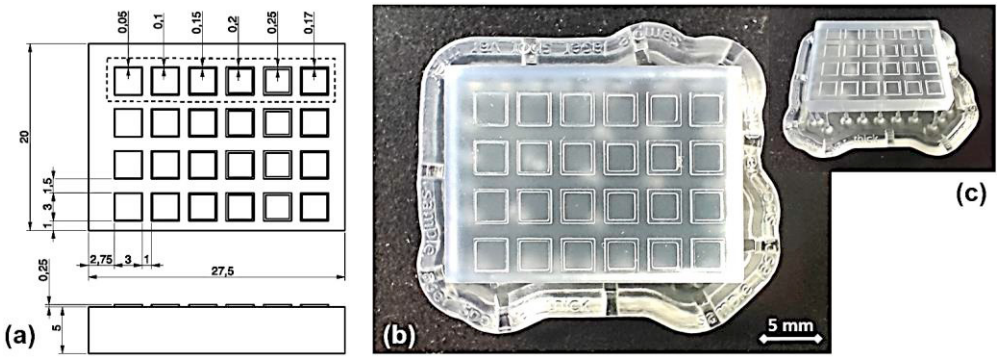

Fig. 7. Test part for the measurement of the correction parameter. Drawing (a); top view (b) and 3D view of the printed part samples (c).

Table 5. Thickness measurement of walls and laser spot diameter estimation.

Thin wall feature	Nominal Thickness	Thickness Along X-axis		Thickness Along Y-axis		Total thickness		Compensation Parameter = Actual D_{LS}
		Average	Error	Average	Error	Average	STD	
#	[μm]	[μm]	[μm]	[μm]	[μm]	[μm]	[μm]	[μm]
1	50	176	126	128	78	152	29	102
2	100	220	120	176	76	198	27	98
3	150	272	122	226	76	249	29	99
4	200	299	99	265	65	282	21	82
5	250	350	100	323	73	337	20	87
6	170	274	104	243	73	258	21	88

Since the path of the laser spot follows the edges of the geometry, the difference between the nominal and the measured wall thickness returns the compensation parameter, according to the hypothesis, likely equal to the actual diameter of the laser beam spot. The measurements are reported in Table 5 with the estimated laser beam spot diameter. The actual laser beam spot diameter (and compensation C) ranges between 88 and 102 μm, with an average value of 93 μm. It must be observed that the average value tends to be greater than the nominal diameter of 85 μm, with a growing trend when the wall thickness is thinner. This latter effect seems to be related to the stepover of the two on-edge laser paths (squares from 1 to 3), which increases when the wall thickness decrease. The high values of standard deviations are attributed to the different infill of the wall when the thickness increases at higher values (squared walls 4, 5, and 6). In fact, in these cases, when the wall thickness is higher than the laser beam spot diameter, the infill strategy is a rectilinear scan oriented with a predefined angle, typically along the machine y-axis. With this evidence (figure 8), all walls oriented along the x-axis are filled with a pattern of parallel lines orthogonal to the wall edge. In contrast, all walls oriented along the y-axis are filled with additional lines along the wall edge.

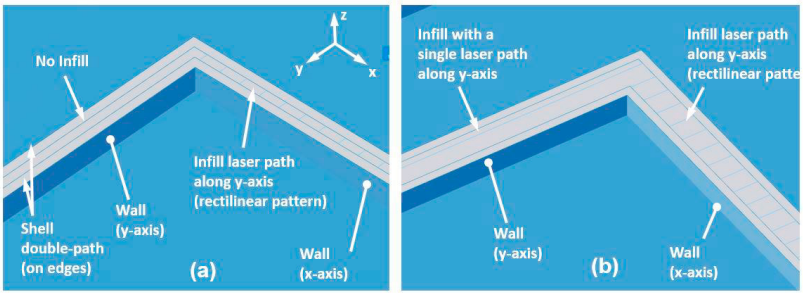

Fig. 8. Laser Spot Path for the wall infill: a) Wall Thickness of 150 μm; b) Wall Thickness of 200 μm.

Therefore, this different curing strategy determines different UV-curing for the same walls with related variable thickness, thus higher values of standard deviations in measurements. Figure 9 reports the graph of measurement of thin wall thicknesses and the estimated laser spot diameter. Nominal values of thin walls are represented by the slanted black dashed line. All deviations from this line are fabrication errors to be quantified. The values of the actual thin wall thicknesses along x- and y-axis are depicted with blue and green solid lines, respectively.

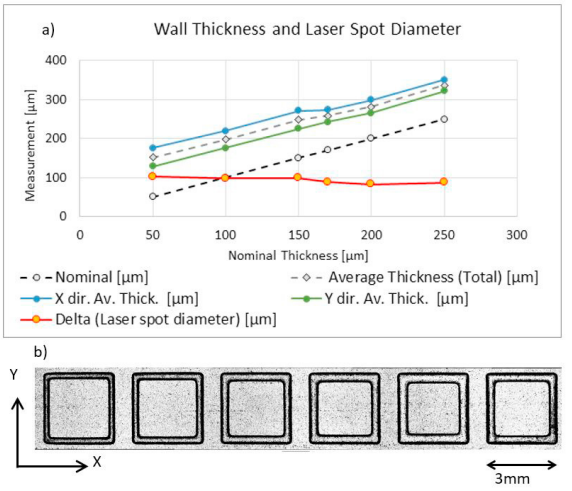

Fig. 9. Measures of thin wall thickness and laser beam spot diameter. (a) Graph of measurements; (b) Image of the profilometer acquisition.

All measured values of thickness are higher than the nominal ones. The average wall thicknesses are depicted with a green dashed line. As can be seen in the figure, wall thicknesses along the x-direction (blue line) are greater than those along the y-axis (green line), but the difference between them decreases beyond the threshold value of t*=150 µm. The difference between measured and nominal values are reported with an orange line. As observed before, the estimated laser beam spot diameter is almost stable to about 100 µm up to the t*, and it decreases to 82-88 µm with thicknesses higher than t*. In fact, as shown, up to t*, the infill is missing along the y-direction while it is always present along the x-direction. The infill strategy significantly impacts wall thickness accuracy. It produces a different wall thickness depending on the wall orientation and nominal thickness, as shown in Fig. 8 and Fig. 9. The error on the thin wall thickness is 74±4.5 µm and 112±11.9 µm along the x- and y-axis, respectively. The graph in Figure 9 shows that the error on the wall thickness along the x-axis is slightly reduced when its value is greater than two times the nominal laser spot diameter. These data suggest that the current infill strategy produces geometrical anisotropy on features. Therefore, the part orientation on the XY plane affects the geometrical accuracy at the micro-scale. A different infill strategy (i.e., following the external perimeter) can improve the geometrical accuracy and reduce the anisotropy.

4. Conclusions

In this study, an SLA process was analyzed in terms of dimensional accuracy addressing micro-feature fabrication by investigating the effect of inaccuracy in laser beam spot diameter and scanning paths. This analysis brought up that the accuracy of the fabrication can be improved by focusing on two aspects: i) the actual value of the laser beam spot diameter, which can be affected by a deviation (up to 10%) from the nominal value; ii) inaccuracy in laser scanning path generation. The first action promoted in this work was a software compensation applied to the part 3D model based on the nominal laser beam diameter, which is 85µm for the used equipment. This method increased the accuracy up to 20% and 30% on micro-pore diameters and depths, respectively. A benchmark test part was then conceived and used to estimate the actual laser spot diameter. This latter investigation revealed that the actual value of the laser beam spot diameter is 93±8 µm, with a deviation from the nominal value of +9.5%. This parameter estimation is crucial to achieve higher accuracy by better calibrating the software compensation. This study has some limitations. It focused

on simple spherical micro-porous structure so that the software compensation is an easy task. It did not consider complex geometries, which can require a challenging assessment to identify the correct compensation. Another relevant limitation is the anisotropy of the compensation parameter since different deviations were measured along different directions. These limitations will be addressed in the future by further investigations. Furthermore, regarding the technology, this study suggests potential improvements in the path generation strategy by compensating the actual laser spot diameter and optimizing the infill algorithm.

Acknowledgments

This work was conceived and developed within the section “Surface treatment and functionalization” REALIZE of the Italian Manufacturing Association AITeM. This work was partially supported by the European Union under the Italian National Recovery and Resilience Plan (NRRP) of NextGenerationEU, partnership on “Telecommunications of the Future” (PE00000001 - RESTART), on “Made in Italy Circular and Sustainable” (PE00000004-MICS) and on “Next generation of sustainable and highly efficient molding processes” Italian Projects of Significant National Interest (PRIN) PNRR 2022 grant n. P2022ZE23N. This manuscript reflects only the authors’ views and opinions, neither the European Union nor the European Commission can be considered responsible for them.

References

[1] Van Der Voort, Pascal, Karen Leus, and Els De Canck (2019) “Introduction to Porous Materials”. *John Wiley & Sons*.
[2] Coussy, O. (2011) “Mechanics and physics of porous solids”. *John Wiley & Sons*.
[3] Netti, Paolo, (Ed.) (2014) "Biomedical foams for tissue engineering applications".
[4] Fang Yin, et al. (2015) "Optically bistable macroporous photonic crystals enabled by thermoresponsive shape memory polymers." *Advanced Optical Materials* 3.11: 1509-1516.
[5] Leo, Sin-Yen, et al. (2017) "Programmable Macroporous Photonic Crystals Enabled by Swelling-Induced All-Room-Temperature Shape Memory Effects." *Advanced Functional Materials* 27.41: 1703522.
[6] Goyal, Bhupesh, and Pandey Akash (2021) "Critical review on porous material manufacturing techniques, properties & their applications." *Materials Today: Proceedings* 46: 8196-8203.
[7] Kafle, Abishek, et al. (2021) "3D/4D Printing of polymers: Fused deposition modelling (FDM), selective laser sintering (SLS), and stereolithography (SLA)." *Polymers* 13.18: 3101.
[8] Bártolo, Paulo Jorge, ed. (2011) “Stereolithography: materials, processes and applications”. *Springer Science & Business Media*.
[9] Zhang, Feng, et al. (2021) "The recent development of vat photopolymerization: A review." *Additive Manufacturing* 48: 102423.
[10] Muldoon, Kirsty, et al.(2022)"High Precision 3D Printing for Micro to Nano Scale Biomedical and Electronic Devices". *Micromachines* 13.4: 642.
[11] Basile Vito et al. (2016) "Analysis and Modeling of Defects in Unsupported Overhanging Features in Micro-Stereolithography." *Proc. of ASME 2016 IDETC-CIE*. Vol. 4. Charlotte, NC, USA. August 21–24, 2016. V004T08A020.
[12] Schmidleithner, Christina, and Deepak M. Kalaskar (2018) "Stereolithography." IntechOpen, 1-22.
[13] Huang, Jigang, Qin Qin, and Jie Wang. (2020) "A review of stereolithography: Processes and systems." *Processes* 8.9: 1138.
[14] Sabbah Aya et al. (2021) "Impact of layer thickness and storage time on the properties of 3d-printed dental dies." *Materials* 14.3: 509.
[15] Arnold, Christin, et al. (2019) "Surface quality of 3D-printed models as a function of various printing parameters." *Materials* 12.12: 1970.
[16] Basile, Vito, et al. (2022) "Micro-texturing of molds via Stereolithography for the fabrication of medical components" *Procedia CIRP* 110:93-98.
[17] Shanmugasundaram Aravind Sunil, et al. (2020) "Mechanical anisotropy and surface roughness in additively manufactured parts fabricated by stereolithography (SLA) using statistical analysis." *Materials* 13.11: 2496.
[18] Cotabarren, Ivana, et al. (2019) "An assessment of the dimensional accuracy and geometry-resolution limit of desktop stereolithography using response surface methodology." *Rapid Prototyping Journal* 25.7: 1169-1186.
[19] Hada, Tamaki, et al. (2020) "Effect of printing direction on the accuracy of 3D-printed dentures using stereolithography technology." *Materials* 13.15: 3405.
[20] Unkovskiy, Alexey, et al. (2018) “Objects build orientation, positioning, and curing influence dimensional accuracy and flexural properties of stereolithographically printed resin”. *Dental Materials*, 34, e324-e333.
[21] Rubayo, David Diaz, et al. (2021) "Influences of build angle on the accuracy, printing time, and material consumption of additively manufactured surgical templates." *The Journal of Prosthetic Dentistry* 126.5: 658-663.
[22] Surace, Rossella, et al. (2021) "Micro Injection Molding of Thin Cavities Using Stereolithography for Mold Fabrication." *Polymers* 13.11: 1848.
[23] Formlabs Materials. Available online: https://formlabs.com/materials/standard/ (accessed on 10 June 2023).
[24] Weaver, Jordan S. et al. (2022) "Laser spot size and scaling laws for laser beam additive manufacturing." *J. of Manuf. Processes* 73: 26-39.